

Proc. 2nd International Symposium on the Effect of Surface Geology on Seismic Motion, Yokohama, Japan, Dec. 1-3, 1998)

Simulations of Long-Period Ground Motions during the 1995 Hyogoken-Nanbu (Kobe) Earthquake using 3D Finite Element Method

Y. Hisada

Dept. of Architecture, Kogakuin University, Japan

H. Bao

Algor Inc., U.S.A.

J. Bielak, and O. Ghattas

Civil and Environmental Engineering Dept, Carnegie Mellon University, U.S.A.

D. R. O'Hallaron

School of Computer Science, Carnegie Mellon University, U.S.A.

ABSTRACT: Long-period strong motions (> 0.9 second) are simulated in the Kobe area for the mainshock (1/17/95) and the aftershock (2/2/95) of the Hyogoken-Nanbu (Kobe) earthquake. In order to model ground motions in the realistic and highly heterogeneous basin structure, an unstructured 3D FEM (Finite Element Method) is used, which runs efficiently on parallel computers. The simulation results show strong 3D basin effects, especially within the disaster belt at the target sites from KBU to RKI.

1 INTRODUCTION

One of the biggest questions during the Kobe earthquake is why the "disaster belt" was created in the Kobe area, where about 6,000 people died and about 200,000 houses were severely damaged. [Fig.1](#) shows the location of the disaster belt, which consists of several narrow strips (about 1 km width) between the Rokko Mountains and the reclaimed lands in front of the Osaka bay. Numerous studies have shown that the large strong motions within the belt were probably caused by a combination of source effects (the forward rupture directivity effects), 2D/3D basin edge effects, and nonlinear effects on the reclaimed lands (e.g., Wald, 1995; Kawase, 1996; Pitarka et al., 1998).

The purpose of this study is to investigate the long-period strong motions (over 0.9 s) in the Kobe area during the 1995 Kobe earthquake using a realistic 3D Osaka basin model. For this, we employ a 3D wavelength-adaptive finite element code, which runs on parallel computers. First, we construct a detailed 3D Osaka basin model, which is based on the recent reflection surveys in the Kobe area. We check the validity of the model by aftershock simulations. Next, we model the Kobe mainshock by three asperities, which reproduce near-field observed records well. Finally, we simulate and discuss the mainshock motions in the Kobe area.

2 3D OSAKA BASIN AND SOURCE MODELING USING 3D FEM

2.1 Construction of the 3D Osaka basin model in the Kobe area

After the Kobe quake, numerous reflection, refraction, and microtremor surveys have been carried out around the Kobe area. [Fig.1](#) shows a detailed contour map for the surface of the Granite basement under the Osaka basin, obtained using the refraction/reflection surveys shown in [Fig.1](#) (Sano, 1998). The surveys indicate that the sediments of the basin mainly consist of four layers: Alluvial /Reclaimed soils, Upper Osaka Group, Middle Osaka Group, and Lower Osaka Group. The surveys also show that the thickness of each sedimentary layer is roughly proportional to the total thickness of the sediments in the Kobe area. Therefore, we calculate each thickness using the average ratios relative to the total thickness down to the basement; the ratios are shown in Table 1. Following Yoshida et al. (1996) and Iwata and Kawase (1997), we model the material properties of the layers within and outside the basin, as shown in Tables 1 and 2.

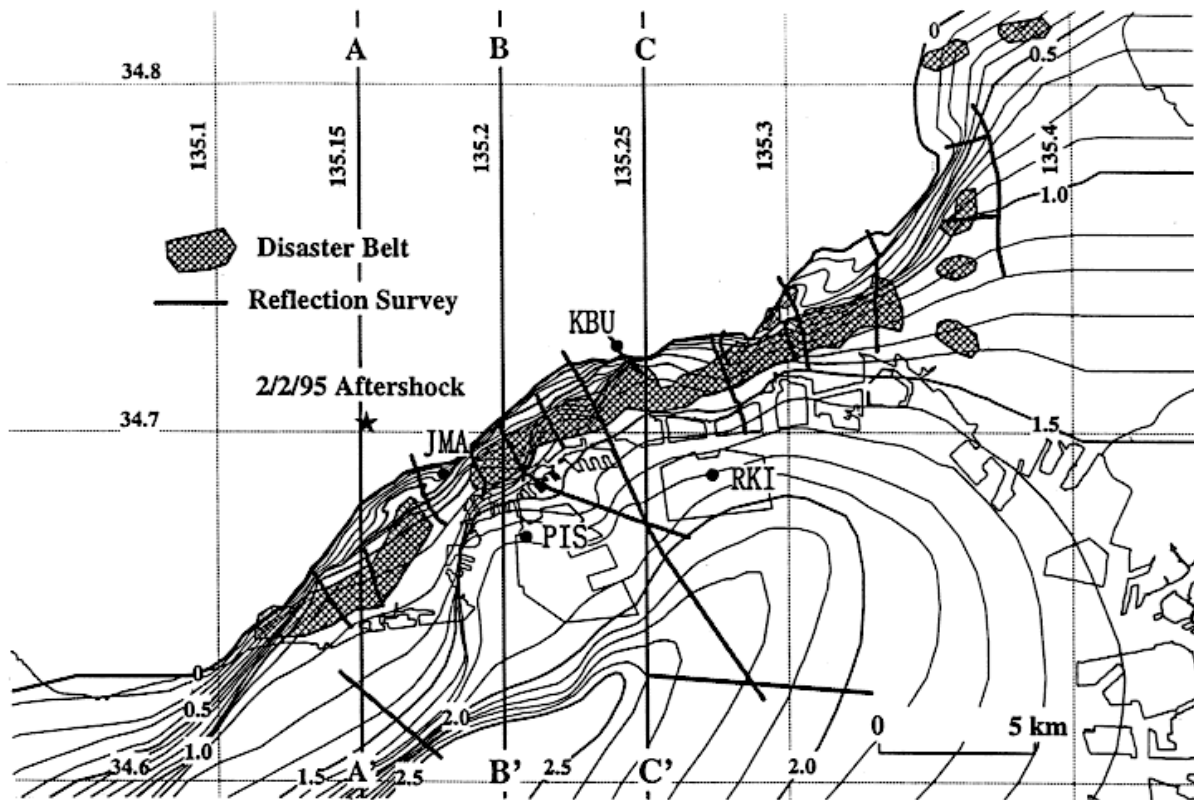


Fig.1 The contours of the Granite basement under the Osaka basin (unit: km), which was made by Sano (1998) using the reflection surveys shown in the figure. The locations of "Disaster Belt", the aftershock, the strong motion sites are also indicated.

[Fig.1](#): The contours of the Granite basement under the Osaka basin (unit: km), which was made by Sano (1998) using the reflection surveys shown in the figure. The locations of "Disaster Belt", the aftershock, the strong motion sites are also indicated.

Table 1: Layered structure under the Osaka basin

("d" is the depth down to the basement at each site)

	Vp	Vs	thick	geological	FE size
g/cm ³	km/s	km/s	km	conditions	km
1.7	1.6	0.4	0.07 x d	alluvial	0.045
1.8	1.8	0.55	0.11 x d	upper Osaka	0.045
2.0	2.0	0.7	0.28 x d	middle Osaka	0.090
2.1	2.5	1.0	0.54 x d	lower Osaka	0.090
2.5	5.5	3.2	5 - d	granite	0.360
2.8	6.0	3.5	-	granite	0.360

Table 2: Layered structure outside the Osaka basin

	Vp	Vs	thick	geological	FE size
g/cm ³	km/s	km/s	km	conditions	km
2.2	3.5	2.0	0.5	weathered	0.180
2.5	5.5	3.2	4.5	granite	0.360
2.8	6.0	3.5	-	granite	0.360

2.2 3D FEM for the Osaka basin, and the introduction of seismic sources

Thus far, structured finite difference methods have been the most widely used for 3D ground motion simulations of complex basins (e.g., Pitarka et al., 1998). Unstructured meshes, on the other hand offer the possibility of tailoring the mesh to the varying wavelengths that arise in the models due to large variations in material properties, such as those shown in Table 1. In the present work we use a parallel elastic wave propagation finite element system developed for modeling earthquake ground motion in large sedimentary basins on parallel computers (Bao et al., 1998). The system, which is built on the parallel unstructured PDE toolset Archimedes, includes the following components: a mesh generator, a mesh partitioner, a parceler, and a parallel code generator, as well as parallel numerical methods for applying the seismic forces, incorporating absorbing boundaries, and solving the discretized elastic wave propagation problem. The mesh size of each element is chosen according to the local properties and maximum frequency of interest, so that the mesh generator produces a well-tailored unstructured mesh. The effectiveness of the numerical methodology and software system have been previously demonstrated in a simulation of the seismic response of the San Fernando Valley in Southern California to an aftershock of the 1994 Northridge earthquake (Bao et al., 1998).

We model the total FE domain including the Kobe area by a cube of 49.68 km x 43.92 km x 36.0 km for the EW, NS, and UD directions, respectively. We generate a FE mesh employing linear tetrahedra. Tables 1 and 2 show standard element sizes in each layer, which was designed to include 7 - 10 elements in the shortest wavelength at the minimum period (0.9 second). The total number of tetrahedra and node points are 44,704,178 and 7,790,694, respectively. Fig.2a, Fig.2b, and Fig.2c show the cross sections of the Vs profile along the longitudinal lines 135.15, 135.2 and 135.25 (see Fig.1); a nearly vertical basin edge can be seen down to about 1.5 km for 135.25, but not for 135.15 and 135.2.

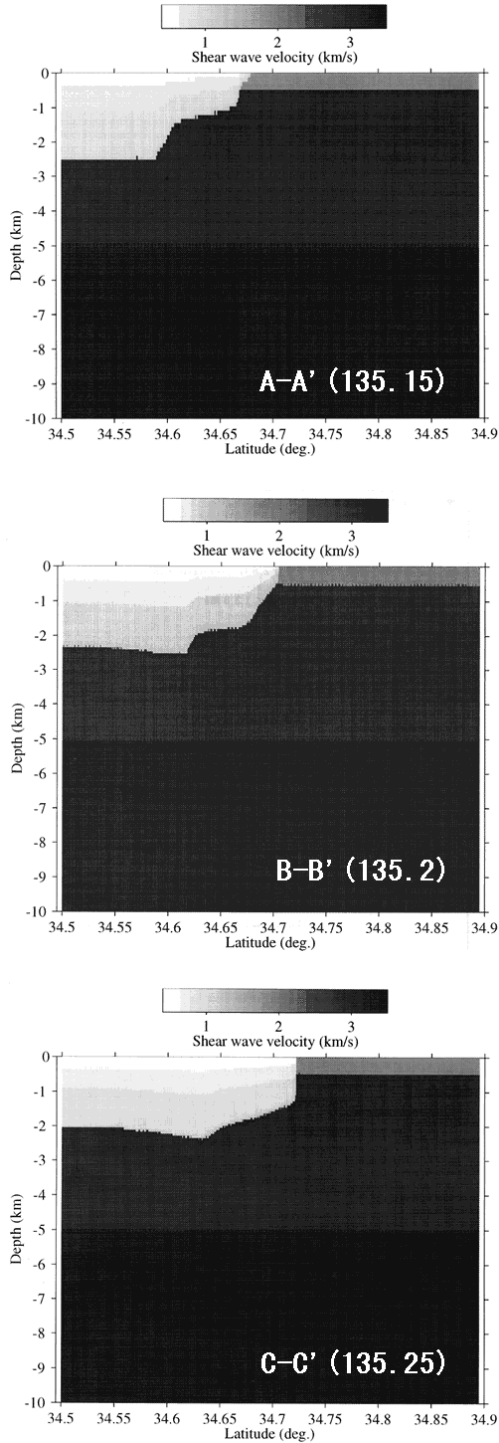


Fig.2: Vs cross-sections along the [A-A'](#), [B-B'](#), and [C-C'](#) lines shown in [Fig.1](#). The smallest and largest Vs are assumed to be 0.4 km/s and 3.5 km/s, respectively, in our model. (see Tables 1 and 2).

Material damping, which is taken to be proportional to the diagonals of the mass element matrix, is included in the model. It varies from $Q=44$ for the layers with a $V_s = 0.4$ km/s to $Q=343$ for materials with $V_s= 3.5$ km/s. First-order absorbing boundaries are introduced at the outside walls and bottom to model the outgoing waves. We introduce the double-couple source in our model using the equivalent forces at the nodes of the element that contains the source (Bao, 1997).

3 RESULTS

3.1 Aftershock (2/2/95) simulation

We check our structure model by comparing the observed records and simulations for the 2/2/95 aftershock ($M_{JMA}=4.2$, see [Fig.1](#)). The source parameters for the aftershock are listed in Table 3 (Iwata, 1997).

Table 3: Source parameters of the 2/2/95 aftershock (Slip velocity is assumed to be an equilateral triangle)

Event	Lat (N)	Lon (N)	Depth (km)	Strike (deg)	Dip (deg)	Rake (deg)	Rise Time (sec)	Starting Time (sec)	Mo (dyne cm)
aftershock	34.703	135.152	17.8	319	74	25	0.2	0.0	1.8×10^{22}

[Fig3-1](#) and [Fig3-2](#) show displacements observed and simulated at the KBU, JMA, PIS, and RKI sites. All the records are band-pass filtered for 0.9 - 5 seconds. For the 1D simulations, we used the theoretical method by [Hisada \(1995\)](#), assuming a 3D wavefield in the 1D flat-layered structure below each site. Since KBU is located outside the basin and on the flat-layered domain, the results between the 1D (GRN) and 3D (FEM) show an excellent agreement. In addition, the waves simulated at KBU successfully reproduce the records. Similarly, the agreement between the 3D simulations at RKI and the observations is excellent. Note, however, that at this site the 1D simulations exhibit large discrepancies with the observations. These results show the validity of our 3D basin model from KBU to RKI, which is our target area. On the other hand, the waves simulated at JMA do not show a very good agreement with the observations for the horizontal components. The vertical component by the 3D simulation is much better than the 1D simulations. This indicates that the source parameters may be not well calibrated for JMA. Similarly, the simulations at PIS do not show a very good agreement with the observations. We may need to modify our preliminary basin model in these areas (e.g., Kawase, 1996; Pitarka et al., 1998).

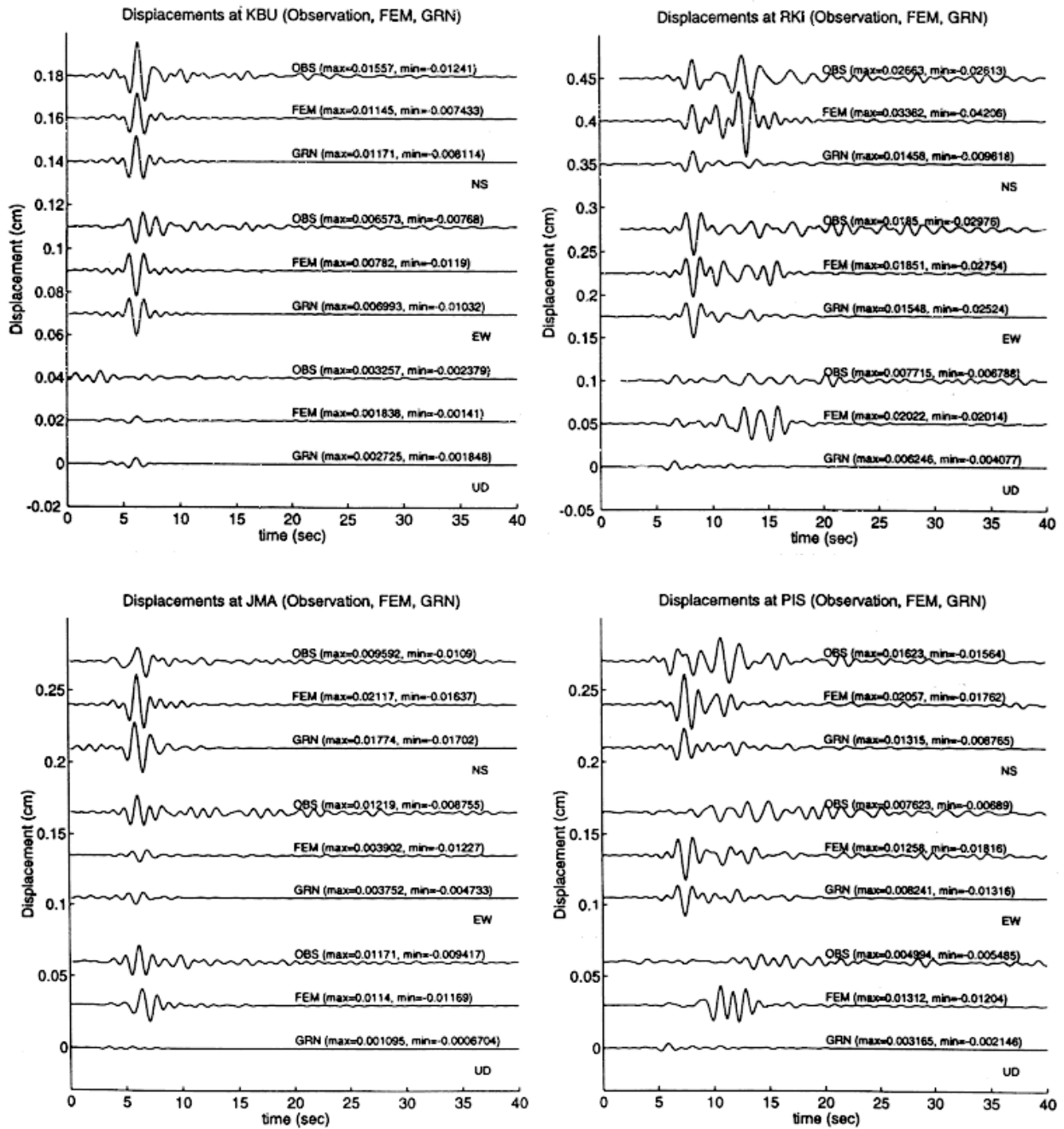


Fig.3 Band-passed displacements (0.9 - 5 sec) observed and simulated for the aftershock at the sites shown in Fig.1. In the figure, OBS, FEM, and GRN indicate the observed records, the simulations by 3D FEM, and by 1D Green's functions, respectively.

[Fig3-1](#) and [Fig3-2](#): Band-passed displacements (0.9 - 5 sec) observed and simulated for the aftershock at the sites shown in Fig.1. In the figure, OBS, FEM, and GRN indicate the observed records, the simulations by 3D FEM, and by 1D Green's functions, respectively.

3.2 Mainshock (1/17/95) simulation

We employ a rather simple source model for the mainshock ($M_{JMA}=7.2$). First, we neglect the Awaji-side fault, because its contribution is negligible to the ground motions in the Kobe area (e.g., Kamae and Irikura, 1998). Second, we model the Kobe-side fault by three point sources shown in [Fig.4](#) and Table 4. Kamae and Irikura (1998) proposed a simple Kobe-side model

consisting of two asperities, which reproduces well the observed strong motions at the KBU and MOT sites (see Fig.4). We extend their model into three asperities in order to reproduce the ground motions not only at KBU and MOT, but also at JMA. Although we need to model the asperities as finite areas to represent the directivity effects, we use the three point sources listed in Table 4, which were confirmed to be equivalent to the finite asperities in our target area.

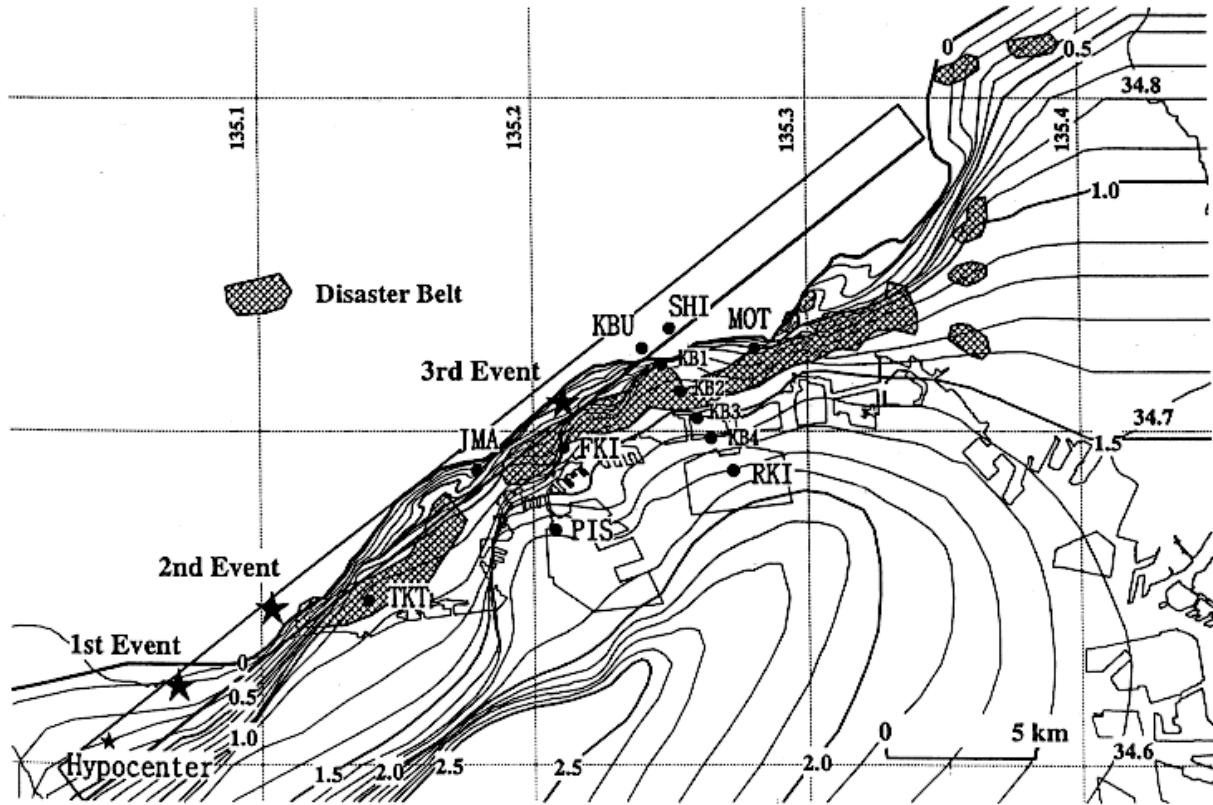


Fig.4 Locations of the three asperities (events) for the Kobe mainshock and observation sites. The basement contours (unit: km) and the disaster belt are also indicated.

Fig.4: Locations of the three asperities (events) for the Kobe mainshock and observation sites. The basement contours (unit: km) and the disaster belt are also indicated.

Table 4: Source parameters of the 1/17/95 mainshock (Slip velocity is assumed to be an equilateral triangle)

Event	Lat (N)	Lon (N)	Depth (km)	Strike (deg)	Dip (deg)	Rake (deg)	Rise Time (sec)	Starting Time (sec)	Mo (dyne cm)
No.1	34.624	135.069	13.051	52	95	210	1.6	1.404	1.098×10^{25}
No.2	34.647	135.104	13.051	52	95	210	1.6	3.178	2.058×10^{25}
No.3	34.709	135.211	7.074	52	95	210	1.6	9.170	1.098×10^{25}

Fig.5-1, Fig.5-2, and Fig.5-3 show velocities recorded and simulated at the sites shown in Fig.4. All velocities are band-pass filtered using a trapezoidal filter with the corners at periods of 0.9, 1,

5, and 10 seconds. As for the aftershock simulations, we also simulated 1D waves using theoretical Green's functions.

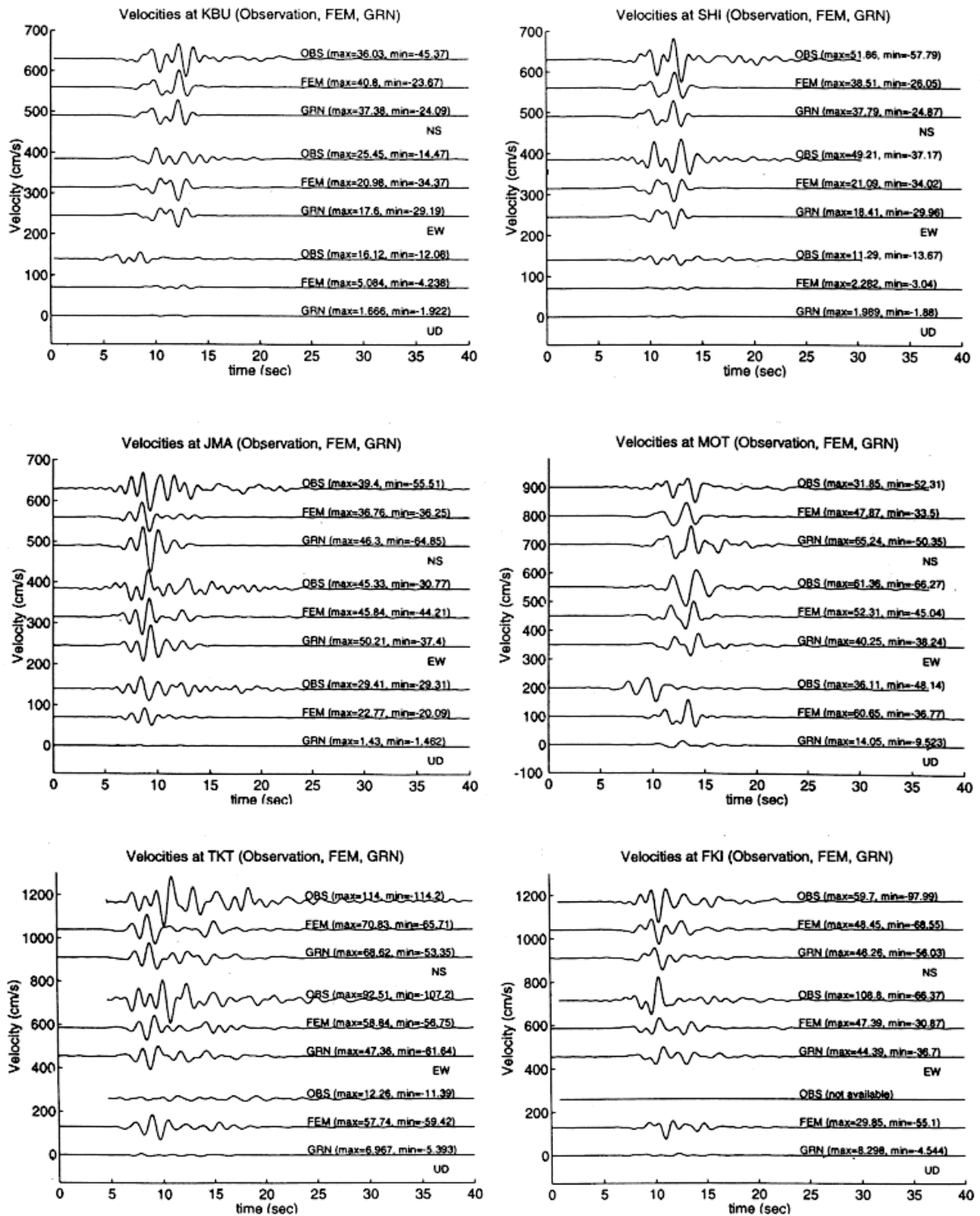


Fig.5 Band-passed velocities (0.9 - 10 sec) observed and simulated for the mainshock at the sites shown in Fig.4. OBS, FEM, and GRN indicate the observed records, the simulations by 3D FEM, and by 1D Green's functions, respectively.

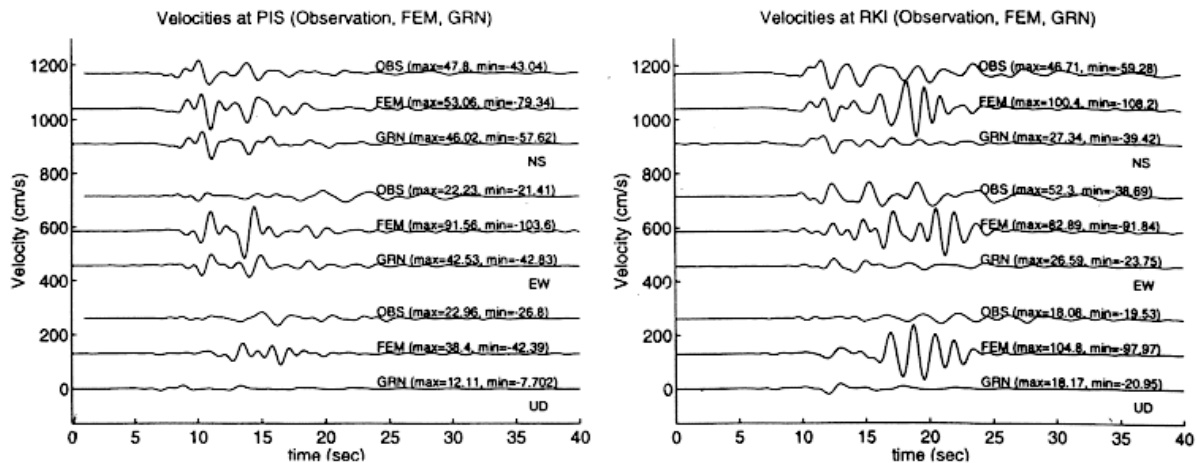


Fig.5 (continued)

[Fig.5-1](#), [Fig.5-2](#), and [Fig.5-3](#): Band-passed velocities (0.9 - 10 sec) observed and simulated for the mainshock at the sites shown in Fig.4. OBS, FEM, and GRN indicate the observed records, the simulations by 3D FEM, and by 1D Green's functions, respectively.

[KBU and SHI](#) are located on the flat-layered region outside the basin. At these locations, observed velocities and those from the simulated waves show excellent agreement. This indicates the validity of our simple source model.

[JMA and MOT](#) are inside the basin, but outside the disaster belt. Since both sites are very close to the basin edge, the horizontal amplitudes of the 3D simulations are smaller than those of the 1D. The vertical amplitudes of the 3D are larger than the 1D, which is similar to the observation at JMA.

[TKT and FKI](#) are about 1 km apart from the basin edge, and are within the disaster belt. We do not see large differences between the 3D and 1D simulations at the two sites, except for the vertical components. The large horizontal amplitudes of the observations are not well reproduced, especially at TKT. As shown in the cross sections along the 135.15 and 135.2 lines in [Fig.4](#), both velocity profiles of our model do not have steep basin edges in this area. That may be one of the reasons why the simulations do not reproduce the large later phases. We may need to modify our preliminary basin model in this area.

[PIS and RKI](#) are more than 2 km apart from the basin edge, and are on reclaimed lands outside the disaster belt. Liquefaction was widely observed at both sites as a consequence of the mainshock. The 3D simulations generate large surface waves, especially at RKI, which exceed the observed level. Since the observed records also show surface waves, but with longer periods, we may need to model the non-linear effects of sub-surface soils in the future.

Finally, [Fig6](#) shows the 3D simulations at KBU, KB1 - KB4, and RKI. Although we do not show each contribution from the three point sources, the waves from the No.2 and No.3 sources are the main contributors to this area. As seen in [Fig.4](#), KB2 is within the disaster belt, and shows the maximum amplitude among the simulations; that is in contrast to the small amplitudes at KB1. This is undoubtedly caused by the constructive interference between the body waves from the basin bottom and diffracted/surface waves from the steep basin edges (the basin edge effects; e.g., Kawase, 1996). As discussed above, the large surface waves at RKI are probably not real.

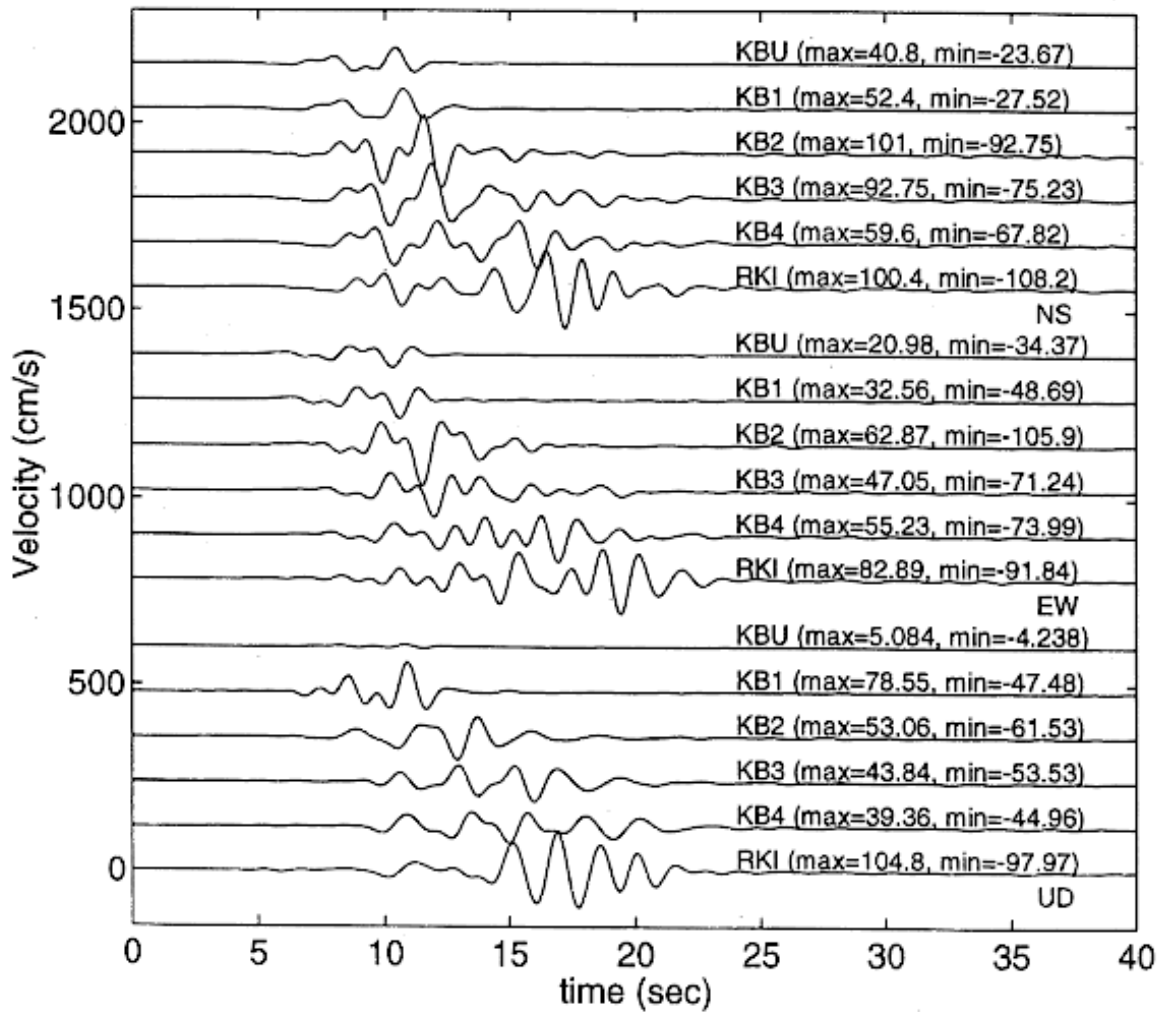


Fig.6 Band-passed velocities (0.9 - 10 sec) simulated by 3D FEM for the mainshock at the target sites shown in Fig.4.

[Fig.6](#): Band-passed velocities (0.9 - 10 sec) simulated by 3D FEM for the mainshock at the target sites shown in [Fig.4](#).

4 CONCLUSIONS

We simulated the long-period strong motions (> 0.9 second) in the Kobe area for the 2/2/95 aftershock and the 1/17/95 mainshock using a realistic 3D Osaka basin model and FEM. Even though our basin model is not highly refined, the simulation showed the validity of our methodology, especially around the KBU-RKI areas. We found strong 3D basin effects, especially large amplifications near steep basin edges and within the disaster belt, and generation and propagation of local surface waves. At the same time we observed that the agreement between observations and results from simulations was poor at other sites. Thus, it appears that improvements in the source and basin models are necessary in order to reproduce the observed response throughout the "disaster belt."

ACKNOWLEDGMENTS

This research was supported by the National Science Foundation's Grand Challenges in High

Performance Computing and Communications program, under grant CMS-9318163, and "US-Japan Cooperative Research for Urban Earthquake Disaster", which is planned as a Special Project of the Ministry of Education, Science, Sports and Culture and the Disaster Prevention Research Institute (DPRI), Kyoto University. Computing services on the Pittsburgh Supercomputing Center's Cray T3E and DEC 8400 were provided under PSC grant BCS-960001P. The data used here is are collected and distributed by Japanese Working Group on ESG (Effects of Surface Geology on Seismic Motion), Association for Earthquake Disaster Prevention, for the Kobe Simultaneous Simulation Project during the second International Symposium on ESG (ESG98) held at Yokohama, Japan, 1998. In addition, the strong motion records from CEORKA (The Committee of Earthq. Obs. And Res. In the Kansai Area), Japan Meteorological Agency, Japan Railway Co. (FD No. R-030), Osaka Gas Co., and Kansai Electric Co. are used.

REFERENCES

- Bao, H. 1997. 3-D FEM Simulation of earthquake ground motion in realistic basin models: Model Implementation and Site Effect Analysis, Ph.D. theses, Comput. Mech. Lab., Civil and Environmental Dept., Carnegie Mellon Univ.
- Bao, H., J.Bielak, O.Ghaffas, L.F.Kallivokas, D.R.O'Hallaron, J.R.Shewchuk, and J.Xu 1998. Large-scale simulation of elastic wave propagation in heterogeneous media on parallel computers, Comput. Methods Appl. Mech. Engrg. Vol.152, 85-102
- [Hisada, H. 1995. An efficient method for computing Green's functions for a layered half-space with sources and receivers at close depths \(Part 2\), Bull. Seism. Soc. Am., Vol.85, 1080-1093.](#)
- Iwata, T. and H.Kawase 1997. Deep underground structure beneath Kobe and Osaka area for simultaneous simulation, ESG98 Material
- Kamae, K. and K.Irikura 1998. Source Model of the 1995 Hyogoken Nanbu earthquake and simulation of near-source ground motion, Bull. Seism. Soc. Am., Vol.88, 400-412
- Kawase, H. 1996. The cause of the damage belt in Kobe: "the basin-edge effect", constructive interference of direct S-wave with the basin-induced diffracted/Rayleigh waves, Vol.67, 25-34
- Pitarka, A., K.Irikura, T.Iwata, and H.Sekiguchi 1998. Three-dimensional simulation of the near-fault ground motion for the 1995 Kobe, Japan, earthquake, Bull. Seism. Soc. Am., Vol.88, 751-767
- Sano, M. 1998. Internal structure of the Osaka basin and blind active faults, Proc. 11th Seminar on Research of Active Faults, 6-23, (in Japanese)
- Wald, D. 1995. A preliminary dislocation model for the 1995 Kobe, Japan, earthquake determined from strong motion and teleseismic waveforms, Seism. Res. Lett., Vol.66, 22-28
- Yoshida, S., K.Koketsu, B.Shibazaki, T.Sagiya, T.Kato, and Y.Yoshida 1996. Joint inversion of near- and far-field waveforms and geodetic data for the rupture process of the 1995 Kobe earthquake, J. Phys. Earth, Vol.44, 437-454